Comptes Rendus

Chimie

Bogdan-Constantin Condurache, Corneliu Cojocaru, Petronela Pascariu, Petrisor Samoila and Valeria Harabagiu

Innovative nanostructured magnetite/wool/polysiloxane composite as magnetic adsorbent for oil spill removal

Active site engineering in nanostructured materials for energy, health and environment /
Ingénierie de sites actifs dans les matériaux nanostructurés pour l'énergie, la santé et l'environnement

Innovative nanostructured magnetite/wool/polysiloxane composite as magnetic adsorbent for oil spill removal

Bogdan-Constantin Condurache[ⓘ] [a], **Corneliu Cojocaru**[ⓘ] [*, a], **Petronela Pascariu**[ⓘ] [a],
Petrisor Samoila[ⓘ] [*, a] **and Valeria Harabagiu**[ⓘ] [a]

[a] Laboratory of Inorganic Polymers, "Petru Poni" Institute of Macromolecular
Chemistry, Aleea Grigore Ghica Voda 41A, 700487 Iasi, Romania

E-mails: condurache.bogdan@icmpp.ro (B.-C. Condurache),
cojocaru.corneliu@icmpp.ro (C. Cojocaru), pascariu_petronela@yahoo.com
(P. Pascariu), samoila.petrisor@icmpp.ro, samoila.petrisor@yahoo.com (P. Samoila),
hvaleria@icmpp.ro (V. Harabagiu)

Abstract. We report herein the synthesis and characterization of a new nanostructured composite (Wool-Fe_3O_4-Polysiloxane) aimed to be applied as a magnetic adsorbent for oil spill cleanup. The synthesized composite was characterized by the physical–chemical instrumental techniques (XRD, FTIR, SEM-EDX, and VSM). The hysteresis loops from the VSM measurement disclosed a magnetic saturation value of $M_S = 5.47$ emu/g that was sufficient to induce magnetic properties to the composite material. The produced magnetic adsorbent showing hydrophobic properties was successfully tested for the sorption of petroleum products. Kinetic data of oily liquids retention and dripping were modeled by using the exponential and hyperbolic regression equations with three parameters. The hyperbolic kinetic model suggested higher maximal sorption capacity at time zero ($t = 0$), that is, 14.486, 12.896, and 3.501 g/g, for motor oils 15W, 5W, and *n*-dodecane, respectively. The advanced recovery (80–92%) of retained oils from the spent sorbent was done by centrifugation.

Keywords. Oil spill sorbent, Magnetic composite, Magnetite Fe_3O_4, Polysiloxane, Retention-dripping kinetics.

Published online: 11 April 2022

1. Introduction

Accidental pollution of waters with hydrocarbons may occur as a result of the extraction of crude oils, or due to the transport and storage of petroleum and its derivative products. Combating oil spill pollution by using physical remediation techniques is a rapid intervention measure that enables the prevention of the advanced dispersion of oily substances into the water bodies [1]. Oil spill cleanup by physical remediation can be accomplished by the utilization of floating booms [1,2], skimmers (oil-collecting devices) [3,4], and sorbent materials [5–9]. From these remediation practices, the use of sorbents rep-

resents the most cost-efficient method, especially for small or constrained polluted areas. In addition, the sorbents can be also applied as the finishing method after the booms and skimmers were employed previously. In the last few decades, special attention was devoted to the development of magnetic sorbents for the collection of oil spills from contaminated waters [10,11]. The advantage of magnetic adsorbents relies on the fact that this type of material can be easily driven and collected after the oil uptake by using an external magnetic field [10]. The utilization of iron oxide nanoparticles (e.g., magnetite Fe_3O_4) for the formulation of adsorbent composites with magnetic properties has attracted increasing attention in the field of nanotechnology and wastewater treatment [11,12]. For instance, several authors [13] developed a magnetically superhydrophobic bulk material (PTFE/CNTs/Fe_3O_4) for oil removal. This composite revealed a moderate oil sorption capacity (0.71 g/g) but showed excellent thermal stability that enabled burning directly the collected oil without major deformation of the bulk material that can be reused. Different research groups produced Fe_3O_4-based composite materials of particulate forms (microstructured and nanostructured) with magnetic properties for oil sorption applications [14–19]. For example, Mao and co-workers [15] synthesized magnetic microspheres based on magnetite (Fe_3O_4) and poly(styrene-co-divinylbenzene) in a polymerization process. These microspheres showed hollow and porous structures beneficial for oil sorption applications [15]. In another work, Reddy *et al.* [19] fabricated two series of polymer-grafted magnetite nanospheres. These authors found that polystyrene grafted Fe_3O_4 nanospheres were better than poly(butyl-acrylate) grafted iron-oxide nanoparticles in terms of oil removal efficiency [19].

Compared to granular adsorbents, three-dimensional (3D) materials (e.g. sponges, foams, and aerogels) demonstrated greater oil sorption capacities owing to their open structures and respectively more developed macroporous capillary systems. In this regard, several research groups [20–23] successfully fabricated magnetic composite sponges for oil spill cleanup applications. In Ref. [20], was reported the preparation of a magnetic superhydrophobic composite by coating the commercial melamine sponges with Fe_3O_4, polydopamine (PDA), and polydimethylsiloxane (PDMS). Polyurethane-based composite sponges loaded with magnetite (Fe_3O_4) were also reported as efficient magnetic sorbents for oil uptake [21–23].

Another important class of oil sorbents implies fibrous materials that can be of synthetic or natural origin. The ultrathin synthetic fibers can be fabricated by using the electrospinning process [24–26]. For instance, Song and co-workers [24] produced by the electrospinning method a magnetic fibrous sorbent (polystyrene–Fe_3O_4) for efficient oil adsorption. Apart from magnetite, spinel ferrites also proved to be valuable magnetic components for preparing fibrous hybrid sorbents by the electrospinning process [25,26]. Regarding the natural fibers (e.g., kapok, cattail, cotton, wool, etc.), these represent attractive biomaterials for developing low-cost oil sorbents [27, 28]. Hence, the development of magnetic composites based on natural fibers is topical and of practical interest.

The objective of this study was to turn the wool coarse fibers (environmental wastes) into a valuable product. Thus, herein we focused on producing a new magnetic composite-sorbent (W-Ma-PSi) for oil spill uptake. This composite material was made of wool fibers (W) loaded with magnetite nanoparticles (Ma) that were covered with a polysiloxane layer (PSi) to induce hydrophobic properties. The produced fibrous composite was methodically characterized by physical–chemical techniques, as well as successfully tested for oil sorption applications. Although the wool fibers were previously employed as oil sorbent, this study reports for the first time a new wool-based composite with magnetic and hydrophobic properties, which is efficient for oil uptake and easy to manipulate. Thus, the proposed procedures described in this paper contribute to the advancement in the field of oil spill sorbents.

2. Materials and methods

2.1. *Materials*

Chemical reagents of analytical grade were used as acquired (without further purification); namely: iron(II) sulfate heptahydrate ($FeSO_4 \cdot 7H_2O$, Sigma-Aldrich); ammonia solution 25% (NH_4OH 25%,

Chemical Company RO); hydrogen peroxide solution (H_2O_2 3%, ChimReactiv, RO); toluene (Sigma-Aldrich); *n*-dodecane (Sigma-Aldrich); ethanol (99.5%, ChimReactiv, RO); octamethylcyclotetrasiloxane (**D₄**), 98% purity, d_4^{20} = 0.9561 g/cm³ (Fluka); linear oligo-hydromethylsiloxane (**L₃₁**), 1.364% active H, d_4^{20} = 0.9977 g/cm³ (Union Carbide, USA); hexamethyldisiloxane, 99.5% purity, d_4^{20} = 0.7636 g/cm³ (Fluka); VIONIT CS 34C acid catalyst—an ion exchange resin based on poly(styrene-divinylbenzene) beads bearing sulfonic groups (Romanian product) (granulation = 0.4–0.7 mm; specific surface = 35 m²·g⁻¹, exchange capacity = 4.2 mval·g⁻¹; porosity = 39.42%); CSTex—a cross-linking catalyst (Romanian product) based on zinc octoate (16% in petroleum ether) envisaged for hydrophobization experiments.

The raw wool of very coarse grade (74 ± 16 μm fiber diameter) was supplied by a regional sheep farm (Vaslui, Romania). After removing solid macroscopic impurities, the raw wool was washed several times in tap water (tempered at 27–30 °C) followed by rinsing with distilled water. Next, the wool fibers were dried in a laboratory oven at 35 °C for 24 h and then stored for further use.

The following petroleum products were employed in this study as test oily liquids, namely, *n*-dodecane (pure liquid hydrocarbon), as well as two commercial motor oils (15W/40 and 5W/40).

2.2. *Preparing of wool-magnetite composite (W-Ma) by in-situ oxidation process*

The wool-magnetite composite was prepared by *in-situ* oxidation–coprecipitation process. To this end, a sample of wool fibers was immersed in an alkali solution (NH_4OH), where *in-situ* oxidation of Fe^{2+} was performed in the presence of hydrogen peroxide (H_2O_2). According to the experimental protocol, two solutions *A* and *B* were firstly prepared as follows.

Solution A. In a beaker, an amount of 5 g of iron (II) sulfate heptahydrate ($FeSO_4·7H_2O$) was dissolved in 50 mL of distilled water at room temperature (approximately 25 °C) under stirring.

Solution B. In a beaker containing 50 mL of distilled water, 6.4 mL of NH_4OH (25%), 10 mL of H_2O_2 (3%), 0.457 g wool fibers were added. The mixture was left

for 1 h at room temperature to ensure a complete contact between solid and liquid phases.

Both solutions (*A* and *B*) were initially heated to around 80 °C. Then, *solution A* was added in small portions over *solution B* and heating process was continued to around 95 °C for 1 h under mechanical stirring. The purpose of conventional heating was to activate the inorganic reaction and to promote the interaction of the resulting magnetic particles with the wool fibers. The pH of the reaction medium was basic, i.e. around pH 11. The process yielded a mixture of free-standing magnetite (Ma) nanoparticles and W-Ma composite fibers. The produced W-Ma composite fibers were taken appart from the reaction medium and washed several times with distilled water to remove sulfate ions. In order to remove the traces of water, the magnetic composites were also washed twice with absolute ethanol, and then dried at room temperature for 24 h. After separation by using an external magnet, the free-standing Ma nanoparticles were submitted to a similar washing and drying process.

2.3. *Hydrophobization of wool-magnetite composite*

First, the synthesis of a hydrophobic polysiloxane copolymer, namely, poly(methylhydro-dimethyl)siloxane (H_1PDMS) was performed *via* the bulk polymerization-equilibration reaction of octamethylcyclotetrasiloxane (**D₄**), linear hydromethylsiloxane (**L₃₁**) oligomer and hexamethyldisiloxane, heterogeneously catalyzed by VIONIT CS 34C. More details regarding this synthesis method can be found elsewhere [29]. The produced hydrophobic copolymer (H_1PDMS) was characterized by GPC, H^1NMR, and additionally the amount of active hydrogen was also estimated by the modified Zerewitinoff method [29]. The results of polysiloxane characterization were: GPC: $\overline{M}_n$ = 1900 (g/mol); $\overline{M}_w$ = 4407 (g/mol); $\overline{M}_w/\overline{M}_n$ = 2.319; ¹H-NMR: 1.2445% H, and 1.1949% H (by Zerewitinoff method).

Second, a hydrophobization solution was prepared by dissolving 3.904 g of polysiloxane copolymer (H_1PDMS) and 0.976 g zinc octoate (CSTex catalyst) in 200 ml of organic solvent (toluene). Then, a sample of the W-Ma composite fibers was immersed into the hydrophobization solution and left for 1 h at

room temperature to ensure a good solid–liquid contact. The W-Ma sample was then removed from the hydrophobic solution, left about 1 min for dripping the excess of organic solvent, and dried in the oven at hot air (95 °C) for about 1.5 h. In the course of the drying process, the solvent was quickly evaporated, and the copolymer (H_1PDMS) was firmly attached to the composite fibers. Hence, the wool-magnetite composite with strong hydrophobic properties (W-Ma-PSi) was produced by coating the fibers with *H*-functional polysiloxane. As-prepared hydrophobic material was then placed in a desiccator and stored for the next studies.

Hence, the hydrophobic W-Ma-PSi magnetic composite was obtained in two steps. The first one supposed *in situ* oxidation–coprecipitation of iron sulfate in the presence of wool fibers. The process generated a mixture of W-Ma composite fibers and Ma free-standing nanoparticles. In the presence of oxidative mixture (H_2O_2 and NH_4OH), the surface of wool was also oxidized adding to the native carboxyl groups newly formed carboxyl and amino groups generated by the oxidation of chain amide bonds. Moreover, cysteine oxide groups (from wool keratin) are expected to result trough the oxidation of the intermolecular disulfide cross-linking bonds. The magnetite nanoparticles are attached to the wool fiber surface by physical and/or coordination bonds involving the functional groups present on either components surfaces or between iron ions and chelating functional groups of wool. In the second step, in order to mitigate the native relatively hydrophilic character of the wool fibers (a shortcoming in using these materials for oil-spill sorption on water surface), the as-obtained W-Ma composite was subjected to the reaction with the polysiloxane containing chain Si–H active functional groups. The adhering mechanism of polysiloxane (H_1PDMS) onto the solid substrates (e.g. fibers) is reported in Ref. [29]. Generally, dipoles of the polysiloxane chain Si–O–Si are aligned in the direction of the solid substrate, while the methyl moieties ($-CH_3$) are densely bundled and directed outside forming a molecular hydrophobic layer. In addition, the condensation process might occur between functional groups of the solid substrate and reactive silanol groups (Si–OH). The latter ones might be formed as a result of oxidation of Si–H groups at elevated temperatures [29]. A suggestive scenario of wool fiber modification is depicted in Scheme 1.

2.4. *Characterization techniques*

Structural features of the free-standing magnetite nanoparticles were evaluated by recording the powder X-ray diffraction (XRD) pattern, in the interval 20° to 70° (2θ) with a scanning rate of 0.02°/s on a Shimadzu LabX 6000 Diffractometer equipped with graphite monochromator and CuKα ($\lambda = 1.540568$ Å) radiation.

The morphology of Fe_3O_4 nanoparticles were inspected by means of Hitachi High-Tech HT7700 Transmission Electron Microscope (TEM), operated at 120 kV accelerating voltage, in high contrast mode. For this purpose, the magnetite nanoparticles were dispersed in ethanol and the resulting mixtures were ultrasonicated for 30 min. Afterward, the as-prepared suspensions were drop casted on carbon coated copper grids (300 mesh, Ted Pella), and dried at 45 °C (under vacuum). The collected micrographs were explored using ImageJ software, and the histogram of particle size distribution was plotted after analyzing about 400 nanoparticles of magnetite.

Fourier-transform infrared (FTIR) spectra of developed materials were recorded by using a Bruker Vertex 70 model FTIR spectrometer.

The fibrous morphology of the developed composites was examined by scanning electron microscopy (SEM) using an (ESCM) Quanta 200 device envisaged also with EDX module. Moreover, the optical microscopy investigations of the sorption phenomena were also performed by using a Conrad USB digital microscope.

The magnetic properties of the produced materials were evaluated at room temperature by using a vibrating sample magnetometer (VSM) of type Lake Shore model 8607. Magnetic measurements were recorded under an applied magnetic field of 25 kOe. Before each experiment, the investigated material was demagnetized in alternating field.

2.5. *Sorption experiments*

The oil sorption tests were carried out by considering the basic instructions reported in the standard ASTM F 726-12 (*Standard Test Method for Sorbent Performance of Adsorbents*). Thus, a sample of the sorbent (wool-magnetite-polysiloxane composite) was immersed in the liquid phase of the petroleum product. Then, the sorbent was left in this liquid for about
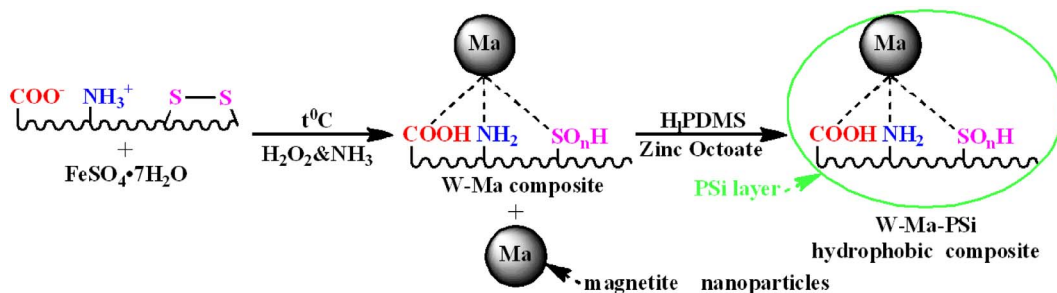
Scheme 1. Chemical modification of the wool fiber surface as a result of *in-situ* oxidation–coprecipitation and hydrophobization processes.

15 min (to ensure the wetting of the solid material). Subsequently, the sorbent loaded with oil was removed from the liquid bath letting it drain for a dripping time equal to 30 s (0.5 min). Finally, the sorbent imbibed with oil was weighed on a digital balance. Hence, the sorption capacity S (g/g) was determined as the ratio between the weight of collected oil and the weight of the dry sorbent, as given by:

$$S = \frac{m_T - m_s}{m_s} = \frac{m_L}{m_s} \qquad (1)$$

where S (g [oil]/g [sorbent]) is the sorption capacity, m_s (g) is the mass of dry (pristine) sorbent sample, m_T (g) is the total mass of the sorbent plus the collected oil, and m_L (g) is the mass of collected oil by the sorbent. Note that in liquids uptake applications the measured sorption capacity depends on the system exposure to the dripping time. Therefore, the sorption capacity is also known as retention capacity in such applications. Gravimetrical measurements for assessing oil sorption capacities were done using a digital balance (KERN) with 0.001 g accuracy. All sorption tests were done at room temperature ($T = 23 \pm 4$ °C).

3. Results and discussion

3.1. *Characteristics of the free-standing magnetite nanoparticles*

Firstly, we assessed some characteristics of Fe_3O_4 nanoparticles that were produced by means of *in-situ* oxidation–coprecipitation process discussed in Section 2.2. The results are shown in Figure 1. Hence, the XRD pattern of the prepared Fe_3O_4 nanoparticles is illustrated in Figure 1a and compared with the standard magnetite JCPDS file no: 19-0629, whereas

the IR-spectrum of the synthetized magnetite is displayed in Figure 1b. From Figure 1a, one may observe a perfect match between the registered and standard patterns. Therefore, the exclusive presence of the diffraction planes typical for pure cubic spinel structure confirms the formation of magnetite, without any detectable secondary phases of iron oxides.

Moreover, based on the registered XRD pattern, the crystallite sizes of the Fe_3O_4 were calculated using the Debye–Scherrer formula (2) considering all diffraction peaks [30,31]:

$$D = \frac{k\lambda}{B\cos\theta} \qquad (2)$$

where D is the crystallite size (nm), k is the shape factor ($k = 0.9$), B is the full width at half maximum of the diffraction peaks (rad), λ is the X-ray wavelength and θ is the Bragg's diffraction angle.

The average crystallite size value for the as-obtained magnetite was 16.9 nm, being in close agreement with previous studies reported in the literature [32].

The XRD observations strongly correlate with the IR spectroscopy data. Thus, the shape of the IR spectrum is typical for magnetite presenting two absorption bands in the range of 600–400 cm^{-1}. As shown in Figure 1b, the band centered at 569 cm^{-1} is associated to the streching vibrations of tetrahedral Fe–O bond and the band at 438 cm^{-1} is assinged to the octahedral Fe–O bond, respectively.

The magnetization versus magnetic field plot registered at room temperature for the obtained magnetite nanoparticles is shown in Figure 2a. The magnetic characterization reveals that the studied sample exhibit a standard ferromagnetic character [33]. Likewise, the saturation magnetization M_S value of 70.64 emu·g^{-1} and the coercivity value of 2.31 Oe are
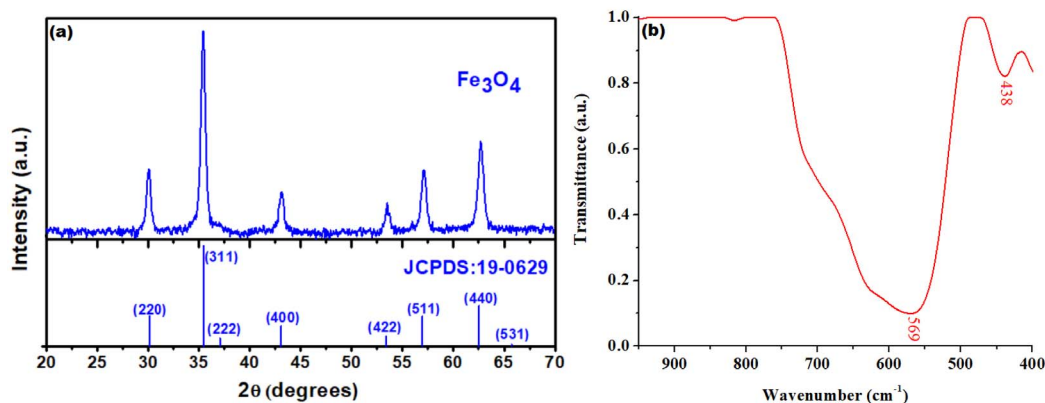
Figure 1. Structural caracterization of Fe$_3$O$_4$: (a) XRD pattern (*versus* standard magnetite (JCPDS:19-0629)) and (b) IR spectrum of nanoparticles synthesised by *in-situ* oxidation–coprecipitation process.

in close agreement with previous reports on magnetite [33,34]. In addition, the morphology of the synthesized Fe$_3$O$_4$ nanoparticles was investigated by using the transmission electron microscopy (TEM). The results of TEM analysis are highlighted in Figure 2(b–d). As one can see from Figure 2b, the produced magnetic nanoparticles are relatively uniform showing mainly spherical or ellipsoidal shapes. Also, the agglomeration tendency is evident owing the magnetic properties of the nanoparticles. The histogram of particle size distribution is shown in Figure 2c, and the cumulative histogram is given in Figure 2d. According to the statistical analysis of collected data, Fe$_3$O$_4$ nanoparticles ranged between 8 and 36 nm in size, implying an average diameter of 19.4 ± 4.9 nm (Figure 2c). As shown by the cumulative histogram (Figure 2d), 90% of the total particles analyzed had a size of less than 26 nm. These findings are in close agreement with previous reports dealing with Fe$_3$O$_4$ synthesis by oxidation–coprecipitation of FeSO$_4$ [34].

3.2. *Characteristics of the fibrous composites*

The morphological and structural characteristics of the produced fibrous composites were investigated by using scanning electron microscopy (SEM) and energy-dispersive X-ray (EDX) spectroscopy. The results of SEM-EDX analysis are summarized in Figure 3.

According to Figure 3a, the fibers of the hybrid material Wool-Fe$_3$O$_4$ show a roughness emerging as

a scales-like pattern (cuticle cells), which is characteristic of wool fibers [28]. By contrast, the fibers of the composite Wool-Fe$_3$O$_4$-Polysiloxane (Figure 3b) do not show the scales-like roughness, suggesting the firm deposition of polysiloxane polymer on the fibers. Likewise, the SEM images revealed fibers diameters of 74–79 μm and 82–97 μm for Wool-Fe$_3$O$_4$ and Wool-Fe$_3$O$_4$-Polysiloxane, respectively. The EDX spectra (Figure 3c,d) disclosed the presence of all expected chemical elements. For instance, the Si element is missing for the hybrid material Wool-Fe$_3$O$_4$ (Figure 3c), but the presence of Si is obvious for the composite Wool-Fe$_3$O$_4$-Polysiloxane (Figure 3d).

In addition, Fourier-transform infrared spectroscopy (FTIR) was employed to evaluate the structure of the magnetic composites. Generally, the purpose of the infrared analysis is to carefully inspect the FTIR spectra to identify the functional groups of the raw material and then compare any structural changes after the modification of the initial material [35]. The FTIR spectra of the composites were compared with those of the precursors (Figure 4).

Figure 4 presents the FTIR spectra of the intermediates as compared of those of wool-magnetite composites. The interpretation of wool spectrum was performed based on available literature information [36–39]. Thus, the following characteristic absorption bands were observed for the wool sample (Figure 4a): a large band centered at 3630 cm^{-1} (O–H vibrations); three bands at 2955, 2922 and 2853 cm^{-1} (C–H vibrations); 1707 and 1688 cm^{-1} (COO$^-$ aspartic and glutamic region); 1661 cm^{-1} (C=O
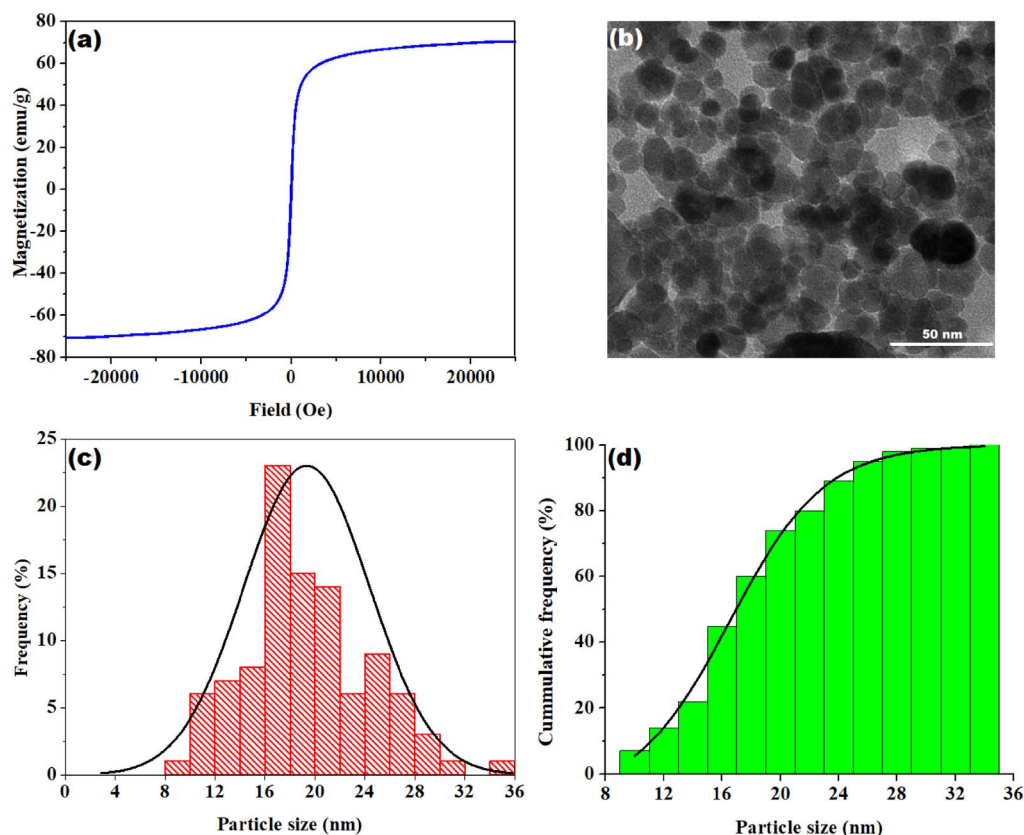
Figure 2. Magnetic and morphological/dimensional caracterization of Fe_3O_4: (a) room temperature hysteresis cycle; (b) representative TEM micrograph; (c) histogram of particle size distribution for magnetite; (d) cumulative histogram of particle size distribution for magnetite.

amide I)—characteristic to secondary structure of wool keratin; 1576 and 1541 cm^{-1} (C–NH amide II); 1229 cm^{-1} (amide III); large bands centered at 1066 and 1040 cm^{-1} (S–O stretching sulfonate, cystine dioxide); very short band attributed to the –S–S– groups at 518 cm^{-1} [39]. Important to note that, even in the native state the wool has the cystine –S–S– bridges partially oxidized. The magnetite characteristic adsorptions were seen as a large band at 569 cm^{-1} (Figure 1b). For W-Ma composite one may see in the insert of Figure 4 the presence of magnetite characteristics bands in the range 617–571 cm^{-1} and the shifting of amide II absorption of wool in the region 1564–1502 cm^{-1}. The modification of both magnetite and amide II characteristic absorptions as compared to the precursors spectra clearly indicate the interactions between the iron oxide and the wool. As previously shown [29] polysilox-

ane reagent used for hydrophobization shows specific bands at 2166 cm^{-1} (Si–H), 1261, 891, 843 and 766 cm^{-1} (Si–CH$_3$ vibrations) and a large band between 1097–1050 cm^{-1} (Si–O–Si) (Figure 4b). The FTIR spectrum of W-Ma-PSi composite (Figure 4c) is more or less a sum of the spectra of individual components. Hence, the bands associated with magnetite are evidently visible within the wavelength range of 600–400 cm^{-1}, but they are shifted to lower frequencies, proving that the polysiloxane interacts with the surface of inorganic particles. The bands attributed to the polysiloxane (1265, 849, 800, 764 and 1090–1036 cm^{-1}) along with shifted bands for aspartic/glutamic acid region (1697 cm^{-1}), amide I (1630 cm^{-1}) and amide II (1558 cm^{-1}) bands of the wool are also present. One should mention that due to the high absorption intensity of Si–O–Si and Si–CH$_3$ bands as compared to those of wool, the in-
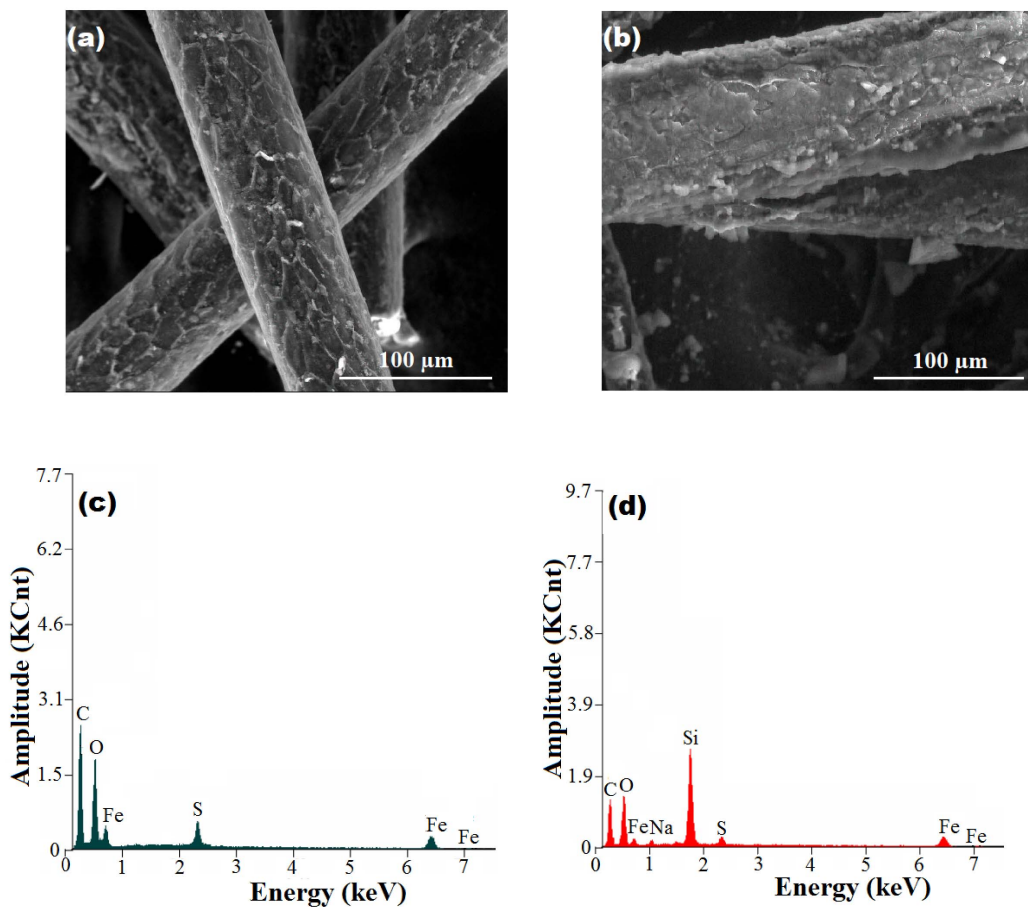
Figure 3. Morphological and structural characteristics of the fibrous composites resulted from SEM-EDX analysis: (a) SEM image of W-Ma fibrous composite; (b) SEM image of W-Ma-PSi fibrous composite (hydrophobic material); (c) EDX spectrum of W-Ma hybrid fiber; (d) EDX spectrum of W-Ma-PSi composite fiber.

tensity of wool bands in the spectrum are much lower than expected considering the wool/polysiloxane ratio in the sample. The Si–H band at 2166 cm^{-1} is still visible in the spectrum of the hydrophobic composite, but of smaller intensity as compared to the H_1PDMS precursor proving only a partial chemical transformation of this functional group during the hydrophobization reaction.

The magnetic properties of the produced composites (W-Ma and W-Ma-PSi) were investigated using the vibrating sample magnetometer (VSM) at 298 K temperature. The loops of the magnetic hysteresis (illustrated in Figure 5) suggested that the prepared composites showed ferromagnetic behaviors. The magnetic parameters such as intrinsic coerciv-

ity (H_C), saturation magnetization (M_S) and remanent magnetization (M_R) were evaluated for each composite from the hysteresis loops. For the hybrid material (W-Ma) the magnetic parameters were found to be $H_C = 4.27 \times 10^{-2}$ Oe, $M_S = 6.79$ emu/g, and $M_R = 0.26$ emu/g. These magnetic parameters are significant since the percent of Fe_3O_4 in the obtained hybrid material (W-Ma) is only 8 wt%. In case of the hydrophobic composite (W-Ma-PSi), the magnetic parameters were somewhat smaller ($H_C = 2.78 \times 10^{-2}$ Oe, $M_S = 5.47$ emu/g, and $M_R = 0.23$ emu/g), but high enough to ensure the magnetic separation from liquid phase. For the latter system containing polysiloxane, the diminishing of the magnetic parameters was compensated by the
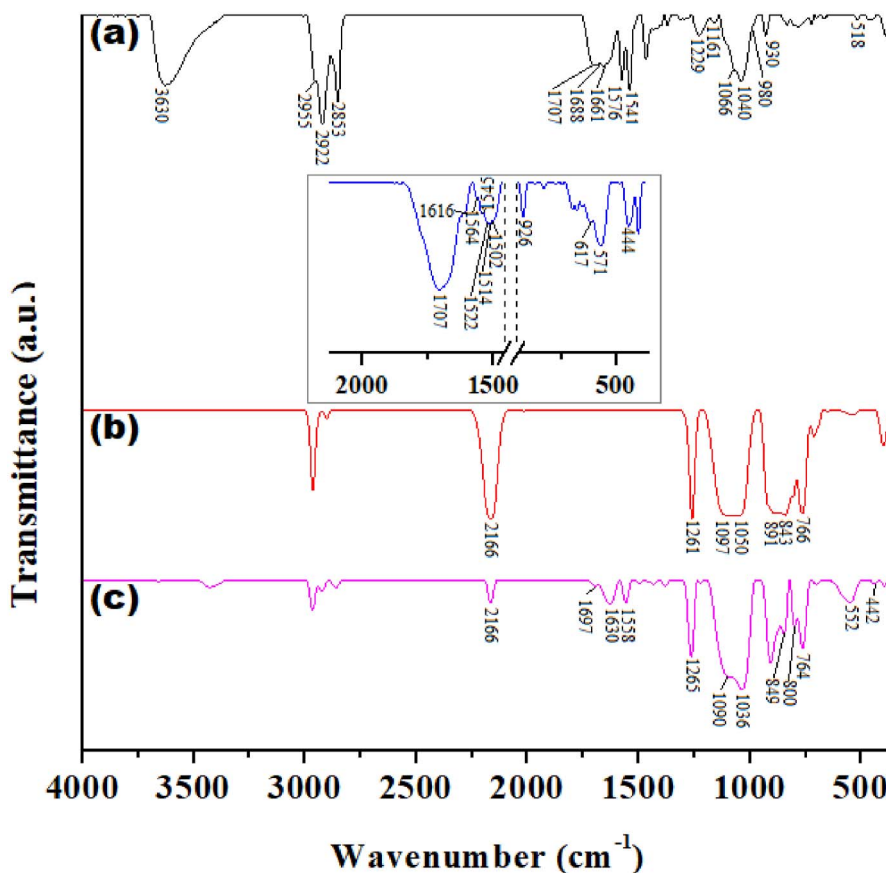
Figure 4. FTIR spectra: (a) Wool fibers; (b) H_1PDMS (polysiloxane); (c) W-Ma-PSi hydrophobic composite; and W-Ma hybrid fibers (insert).

inducing of the superhydrophobic feature to the final product. The wetting properties of the fabricated composites are highlighted in the insert images given in Figure 5 by showing the shape of water droplets on the surfaces of the fibrous samples. For the sample W-Ma (Figure 5, top inset) the water contact angle (WCA) was found to be 52° ± 5°, suggesting a preponderantly hydrophilic surface. Instead, for the sample W-Ma-PSi (Figure 5, bottom inset), the water contact angle was equal to 152° ± 3°, unveiling a superhydrophobic surface.

3.3. *Oil sorption capacity and dripping-retention profiles*

The studied materials (W, W-Ma, and W-Ma-PSi) were first tested as the sorbents for liquids uptake. In this regard, three petroleum products (dodecane,

motor oil 5W, and motor oil 15W) were tested as oily liquids for evaluation of sorption capacity. The main characteristics (density, viscosity, and surface tension) of tested oily liquids are summarized in Table 1. As highlighted in Table 1, the tested oily liquids disclosed moderate differences in surface tension and density, but large difference in viscosities. A comparison between the performance of the raw wool (W) and modified wool fibers (W-Ma and W-Ma-PSi) for liquids uptake is reported in Figure S1 from *Electronic Supporting Information* (ESI). According to the results reported in Figure S1 (ESI), the addition of magnetite (Fe_3O_4) particles to the wool fibers diminished the adsorption capacity of the fibrous materials (W-Ma and W-Ma-PSi). This might be explained by the fact that the addition of Fe_3O_4 particles could reduce the spaces between fibers leading to lower liquid uptake. Of course, the objective of using Fe_3O_4
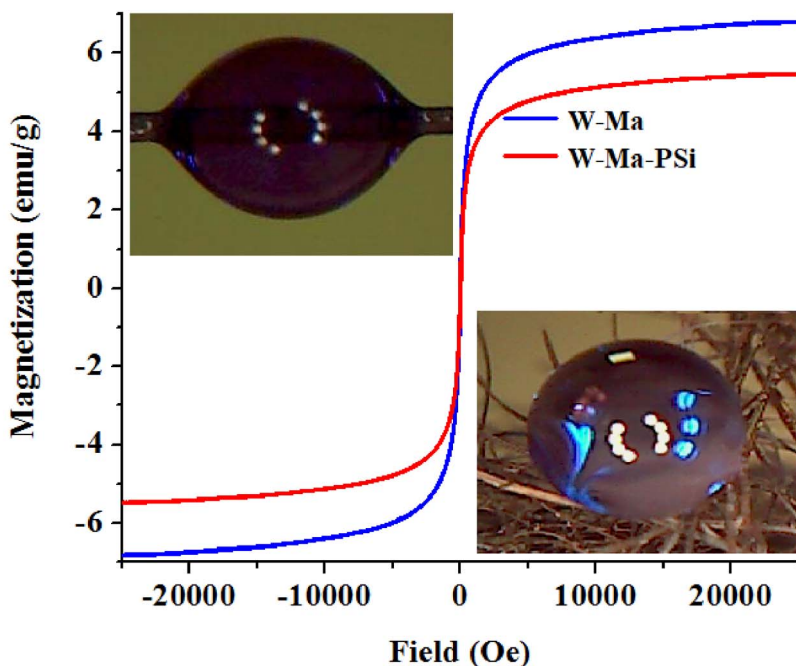
Figure 5. Characteristics of the prepared magnetic composites: (main graph) hysteresis loops derived from VSM measurements; (insets) micrographs showing the wetting properties of the composite materials: (top inset) water droplet onto the surface of W-Ma hybrid fiber; and (bottom inset) water droplets onto the surface of W-Ma-PSi fibrous composite.

Table 1. Characteristics of oily liquids used for sorption tests

Test liquid	Density (g/cm^3) (at 20 °C)	Viscosity (cP) (at 20 °C)	Surface tension (mN/m) (at 20 °C)
n-Dodecane	0.75	1.5	25.3
Motor Oil 5W/40 (MO-5W)	0.85	133.4	29.4
Motor Oil 15W/40 (MO-15W)	0.88	278.8	24.5

nanoparticles was to induce magnetic properties to the final composite material, in order to facilitate the recovery of the spent sorbent from the liquid phase in the presence of an external magnet. Also, it should be pointed out here that the sorption capacities for oils were almost the same for W-Ma and W-Ma-PSi materials (Figure S1). But the water uptake was obviously lower for W-Ma-Psi, suggesting the enhancement of hydrophobic properties by the addition of polysiloxane to the wool fibers.

During the collection of oil, the loaded sorbent is usually subjected to handling and transfer operations. Consequently, the oil retained in large spaces between fibers ("macropores") can be drained under the gravitational force for a given period of time. In this case, the drainage flow rate is influenced by the structural and morphological features of the sorbent as well as by the properties of the oily liquid. Hence, it is essential to determine the kinetics profiles of the retention-dripping phenomena for the studied systems (sorbent-oils) [40]. For our systems of interest (Wool-Fe$_3$O$_4$-Polysiloxane/oils), the experiments for determining the retention kinetics profiles were carried out according to the methodology previously reported [28,40]. To assess kinetics profiles of the retention-dripping process, we determined the re-

tention capacity against the dripping time, as given by [28]:

$$S(t) = \frac{m_T(t) - m_S}{m_S} = \frac{m_L(t)}{m_S} \quad (3)$$

where $S(t)$, denotes the retention capacity, i.e., the amount of oil retained by the sorbent when the whole system (sorbent + oil) is exposed to the dripping time, t (min); m_s is the mass of the sorbent sample, $m_T(t)$ is the total mass of the system (sorbent + oil) determined at the dripping time (t), and $m_L(t)$ is the mass of retained oil by the sorbent at the dripping time (t). Thus, the kinetics of the retention profiles was recorded for the time period ranging from 0.5 to 30 min, that is, $0.5 \leq t \leq 30$. Additionally, the normalized retention R_t was also evaluated as follows [28]:

$$R_t = \frac{S(t)}{S(t_\alpha)} \quad (4)$$

where, $S(t)$ designates here the retention capacity recorded at any given time ($0.5 \leq t \leq 30$ min), and $S(t_\alpha)$ denotes the initial retention capacity recorded in the first moments, that is, the initial retention determined for a dripping time equal to $t_\alpha = 0.5$ min.

The kinetics profiles of the retention-dripping process are given in Figure 6, where the dynamics of retention of oils (dodecane, MO-5W, and MO-15W) by the composite adsorbent (Wool-Fe$_3$O$_4$-Polysiloxane) is shown. These kinetic curves are detailed in terms of actual retention (Figure 6a) and normalized retention (Figure 6b). The collected experimental data were subjected to nonlinear regression analysis in order to compute the parameters of the *unsteady-state model of retention* proposed Bazargan and collaborators [41]. The unsteady-state model proposed in Ref. [41] describes an *exponential decay* of the retention capacity *versus* dripping time. Hence, this exponential model of retention decline can be presented as the actual equation or the normalized equation, as given by [41]:

$$S(t) = S_L \times e^{-k \times t} + S_E \quad \text{(actual equation)} \quad (5)$$

$$R_t = R_L \times e^{-k \times t} + R_E \quad \text{(normalized equation)} \quad (6)$$

where, S_L and R_L denote the model parameters associated with retention-lost due to dripping, (actual and normalized value, respectively); S_E and R_E designate the parameters associated with the retention at equilibrium, (actual and normalized value, respectively); t is the dripping time. The parameter k is the dripping rate constant, which also indicates the arching of the kinetic curve [28,41].

For the studied systems (W-Ma-PSi/oils), the parameters of the unsteady-state model were calculated by nonlinear regression and are summarized in Table 2. Additionally, the *chi-square* statistical test (χ^2 value) was also computed to estimate the goodness-of-fit (Table 2). The lower χ^2 value is, the better is the data interpolation.

A utile characteristic of *the unsteady-state model* of retention [41] is related to the fact that by summing the model parameters S_L and S_E, one can evaluate the maximal sorption capacity at dripping time equal to zero, i.e. $t = 0$ (the boundary condition). Thus, according to the equation of exponential decline of the retention, the sum of the regression parameters ($S_L + S_E$) can approximate the maximum sorption capacity in the initial point, that is, at dripping time zero.

In our case, when the composite material (W-Ma-PSi) was employed as the oil sorbent, the observed initial sorption capacity (determined experimentally at $t = 0.5$ min) was found to be 12.08, 11.24, and 3.43 g/g for MO-15W, MO-5W, and n-dodecane, respectively. Instead, by summing the parameters ($S_L + S_E$) of the exponential decay model, the maximal sorption capacity was estimated to be 12.745, 12.034, and 3.447 g/g, for MO-15W, MO-5W, and n-dodecane, respectively (see Table 2). In that manner, the sum of two regression parameters ($S_L + S_E$) can extrapolate the initial sorption capacity (at $t = 0$), thereby offering valuable information for the studied system (sorbent–oil).

According to Table 2, the greatest *dripping-rate constant* ($k = 0.278$) was found for the motor oil (MO-15W), which has the highest density. Instead, the smallest value for the dripping-rate constant ($k = 0.160$) was found for n-dodecane, which has the lowest density. Hence, results revealed that the heaviest oily liquid MO-15W was drained somewhat quicker than MO-5W, and much faster than n-dodecane (Figure 6). Similar results were reported for the case when the pristine wool sample was used as the oil sorbent [28]. Experimental data disclosed that n-dodecane (the least density liquid) was better retained by the fibrous composite material through capillary forces. Therefore, in the case of n-dodecane, the equilibrium (steady-state) was reached faster approximately in 5 min (Figure 6). By contrast, the heavier motor oils (MO-15W and MO-5W) continued to drip even after 5 min, approaching the steady-state
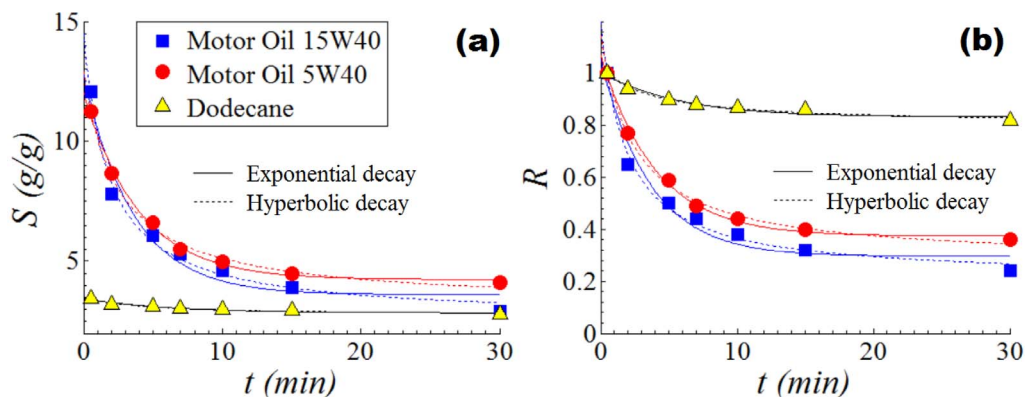
Figure 6. Kinetics profiles of the retention-dripping process showing the dynamics of oil retention onto the composite sorbent (W-Ma-PSi): (a) actual profiles; (b) normalized profiles; solid and dot lines—predictions given by mathematical models.

Table 2. Kinetic models and parameters applied to analyze the oil dripping-retention profiles for the sorbent W-Ma-PSi

Kinetic models and parameters	Type of oil (oily liquid tested)		
	Motor Oil 15W/40 (MO-15W)	Motor Oil 5W/40 (MO-5W)	Dodecane
Exponential decay (actual equation) $S(t) = S_L \times e^{-k \cdot t} + S_E$	$S_L = 9.132$ g/g $S_E = 3.613$ g/g $S_L + S_E = 12.745$ g/g $k = 0.278$ min^{-1} $\chi^2 = 3.652 \times 10^{-1}$	$S_L = 7.795$ g/g $S_E = 4.239$ g/g $S_L + S_E = 12.034$ g/g $k = 0.252$ min^{-1} $\chi^2 = 1.201 \times 10^{-1}$	$S_L = 0.595$ g/g $S_E = 2.852$ g/g $S_L + S_E = 3.447$ g/g $k = 0.160$ min^{-1} $\chi^2 = 2.601 \times 10^{-3}$
Exponential decay (normalized equation) $R(t) = R_L \times e^{-k \cdot t} + R_E$	$R_L = 0.759$ $R_E = 0.295$ $k = 0.276$ min^{-1} $\chi^2 = 2.940 \times 10^{-2}$	$R_L = 0.695$ $R_E = 0.374$ $k = 0.250$ min^{-1} $\chi^2 = 1.180 \times 10^{-2}$	$R_L = 0.171$ $R_E = 0.832$ $k = 0.175$ min^{-1} $\chi^2 = 8.761 \times 10^{-4}$
Hyperbolic decay (actual equation) $S(t) = \dfrac{S_A \times \beta}{\beta + t} + S_B$	$S_A = 11.899$ g/g $S_B = 2.587$ g/g $S_A + S_B = 14.486$ g/g $\beta = 1.848$ min $\chi^2 = 9.969 \times 10^{-2}$	$S_A = 9.734$ g/g $S_B = 3.162$ g/g $S_A + S_B = 12.896$ g/g $\beta = 2.504$ min $\chi^2 = 2.888 \times 10^{-2}$	$S_A = 0.748$ g/g $S_B = 2.753$ g/g $S_A + S_B = 3.501$ g/g $\beta = 4.360$ min $\chi^2 = 1.075 \times 10^{-3}$
Hyperbolic decay (normalized equation) $R(t) = \dfrac{R_A \times \beta}{\beta + t} + R_B$	$R_A = 0.987$ $R_B = 0.209$ $\beta = 1.888$ min $\chi^2 = 7.569 \times 10^{-3}$	$R_A = 0.869$ $R_B = 0.277$ $\beta = 2.539$ min $\chi^2 = 2.348 \times 10^{-3}$	$R_A = 0.216$ $R_B = 0.805$ $\beta = 3.885$ min $\chi^2 = 3.497 \times 10^{-4}$

after 15 min (Figure 6). Notice that, there is a slight difference between the dripping-rate constants calculated from the actual equation and from the normalized one (see Table 2). This small difference might be attributed to the data conversion from the actual to the normalized scale.

It should be mentioned herein that according to the regression equation library, the unsteady-state

model of retention is identical to the regression equation of three-parameter single-exponential decay.

In addition, by making use of the regression equation library, we interpolated the experimental data of unsteady-state retention by using the hyperbolic regression equation with three parameters. We employed this hyperbolic equation by assuming the fact that the retention can be expressed also as being inversely proportional to the dripping time. Hence, the hyperbolic regression model (*three-parameter hyperbolic decay*) can be expressed as follows (in terms of actual and normalized equations):

$$S(t) = \frac{S_A \times \beta}{\beta + t} + S_B \quad \text{(actual equation)} \tag{7}$$

$$R(t) = \frac{R_A \times \beta}{\beta + t} + R_B \quad \text{(normalized equation)} \tag{8}$$

where, β, S_A, S_B, R_A, and R_B are regression parameters of the adopted hyperbolic decay model.

These parameters were calculated by the non-linear regression method and were also reported in Table 2 along with the corresponding *chi-square* statistical test (χ^2 value). According to the data summarized in Table 2, the hyperbolic decay model provided a better prediction than the exponential decay model, owing to smaller χ^2-values. In addition, the three-parameter hyperbolic decay model also allows extrapolating maximal sorption capacity at dripping time zero. Hence, by assuming $t = 0$ in the hyperbolic model, the maximal sorption capacity can be estimated as the sum of the regression parameters ($S_A + S_B$). As reported in Table 2, the maximal sorption capacity estimated by the hyperbolic model ($S_A + S_B$) was equal to 14.486, 12.896, and 3.501 g/g, for MO-15W, MO-5W, and *n*-dodecane, respectively. The maximum absorption capacities estimated by the hyperbolic model proved to be higher than those extrapolated by the exponential model (see Table 2).

At the end of the retention dynamics test, the spent sorbent was subjected to centrifugation in order to recover in the advanced fashion the remained oily liquid, which was not possible to be recovered by simple draining under the gravitational force. The centrifugation experiments were done for 1 min at 2000 rpm. The total efficiency was found to be 92.41± 0.89% for recovery of motor oils and 80.35 ± 0.30% for recovery of *n*-dodecane from the loaded sorbents. Moreover, the recycling of the wool-based sorbent (W-Ma-PSi) was tested in five cycles of use (or four

cycles of reuse), see Figure S2 from *electronic supporting information* (ESI). After each sorption assay, the retained oil was recovered by centrifugation (at 2000 rpm), and the recycled sorbent was reused in the next test. Results revealed that in the four cycles of reuse, the adsorbent remained to some extent competitive in terms of sorption performance while keeping its magnetic property. The slightly diminished sorption performance of the recycled sorbent compared to the pristine one might be attributed to the fact that by centrifugation the fibrous-porous morphology of the materials could be partially compressed (Figure S2/ESI).

The application of the fabricated sorbent (W-Ma-PSi) to remove a motor-oil slick from the water surface was also investigated. The results are depicted in Figure 7 by presenting the taken photos and a micrograph. In these experiments, the motor oil was colored by adding the hydrophobic dye Sudan IV (Sigma-Aldrich) in order to induce more contrast (Figure 7a, b, f).

According to Figure 7c–e, the developed composite material (W-Ma-PSi) was responsive under the action of the external magnetic field. This property improved the application of the composite material as an oil spill sorbent by facilitating its manipulation during the cleanup process. The optical microscopy analysis of the recycled sorbent (Figure 7g, h) disclosed the residual oil fractions strongly trapped into the fibrous matrix of the composite. These residual oil fractions (see the encircled and squared zones in Figure 7h) were trapped in the form of oil bridges between fibers being retained by very strong capillary forces.

Finally, Table 3 compares the oil spill sorbent (W-Ma-PSi) obtained in this study with other magnetic sorbents reported in the literature. The oil sorption performance for the composite reported in this work is in-between if compared with other magnetic materials. But its production cost might be much lower than the composites obtained based on the synthetic polymer matrices. This supposition can be sustained by the fact that the very coarse wool fibers represent low-cost materials (problematic wastes) that need to be turned into useful products. And, the way of valorization of wool wastes presented herein can be seen as an alternative solution to address this issue.
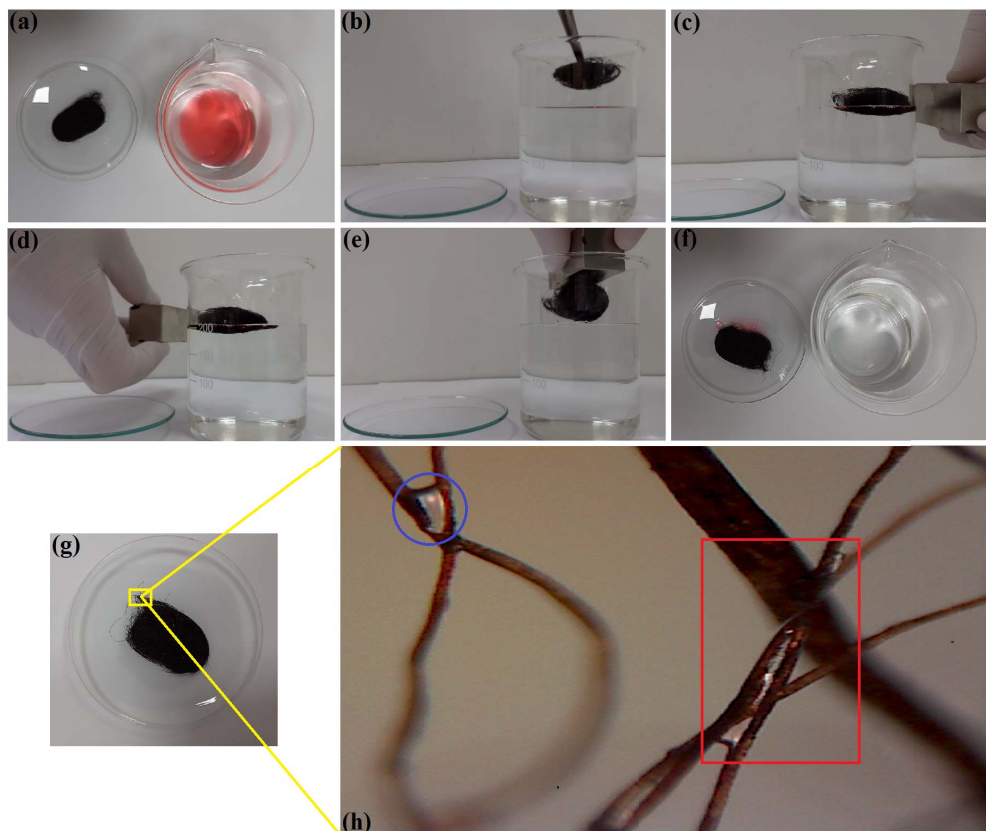
Figure 7. Photo-images showing the application of the composite W-Ma-PSi for the uptake of motor oil (MO-5W) slick from the surface of water: (a, b) pre-sorption: sorbent sample (magnetic fibrous composite) and oil/water system (Sudan IV dyed MO-5W slick on the water surface); (c, d) displacement of the sorbent sample under the action of the applied external magnetic field; (e) removing of the sorbent from the liquid phase under the action of the magnet; (f) spent sorbent (left) and purified water phase (right) after separation, (g) recycled sorbent after centrifugation; (h) micrograph showing the residual fractions of oil trapped at the intersections between fibers of the recycled sorbent through the centrifugation (zoom-in image).

4. Conclusions

In this paper, the raw wool (very coarse fibers, 74 ± 16 µm in diameter) that represents a problematic waste was turned into a magnetic composite with proper morphology for oil sorption. First, a wool-magnetite hybrid material was prepared by an *in-situ* oxidation–coprecipitation process, where the formed Fe_3O_4 nanoparticles (of size 8–36 nm) were attached to the wool fibers. Second, the hybrid fibers were additionally covered with a thin layer of polysiloxane in order to obtain a composite material (Wool-Fe_3O_4-Polysiloxane) with strong hydrophobic properties suitable for oil sorption applications. Ultimately, the produced composite (Wool-Fe_3O_4-Polysiloxane) was well-characterized by means of the advanced physical–chemical instrumental techniques (XRD, FTIR, SEM-EDX, and VSM). The VSM measurements indicated a magnetic saturation value equal to $M_S = 5.47$ emu/g, which was sufficient to allow the withdrawal of the loaded sorbent from the liquid phase by using an external magnet. The water contact angle (WCA) measured for this material (Wool-Fe_3O_4-Polysiloxane) was equal to $152° \pm 3°$, revealing a superhydrophobic surface of the obtained composite fibers.

Table 3. Comparison of different magnetic sorbents in terms of oil sorption capacities

Magnetic sorbent (composite/hybrid material)	Material form	Oil type/ hydrocarbon	Sorption capacity (g/g)	Ref.
PTFE/CNTs/Fe_3O_4	Bulk material	Hexadecane	0.7	[13]
Coco-peat/Fe_3O_4	Powder	Machine oil	5.5	[14]
Poly(styrene-co-DVB)/Fe_3O_4	Microspheres	Diesel oil	4.6	[15]
Polystyrene/Fe_3O_4	Nanoparticles	Diesel oil	2.5	[16]
Fe_3O_4@SiO_2@MPS(methacrylate)	Nanoparticles	Crude oils	17–48	[17]
Poly(oxypropylene)/Fe_3O_4	Microparticles	Crude oils	5–8	[18]
Polystyrene grafted Fe_3O_4	Nanospheres	Gasoline	2.2	[19]
Melamine-PDA-PDMS-Fe_3O_4	Sponge	*n*-Hexane	52	[20]
Polyurethane-Fe_3O_4@OA@GO	Sponge	Kerosene	85	[21]
Polyurethane-PDA-Fe_3O_4-Ag	Sponge	Diesel oil	30	[22]
Polyurethane/Fe_3O_4	Sponge	Pump oil	25	[23]
Polystyrene/Fe_3O_4	Fibrous	Edible oil	87	[24]
Polysulfone/$NiFe_2O_4$	Fibrous	Motor oil	15	[25]
PVDF/$CoFe_2O_4$	Fibrous	Motor oil	18	[26]
Wool-Fe_3O_4-Polysiloxane	Fibrous	Motor oils	11–12	This work

The produced magnetic composite (Wool-Fe_3O_4-Polysiloxane) was tested for the sorption of three petroleum products, namely, *n*-dodecane and two motor oils (MO-15W and MO-5W). The initial sorption capacity was evaluated by exposing the loaded sorbent (i.e., sorbent + oil) to a dripping time of 0.5 min (according to ASTM F 726-12) and it was found to be 12.08, 11.24, and 3.43 g/g for MO-15W, MO-5W, and *n*-dodecane, respectively. In addition, the dynamic of oil retention was also assessed by recording the kinetics profiles of the retention-dripping process for a longer dripping time, of up to 30 min. The experimental data regarding the retention-dripping profiles were interpolated by using the exponential decay and the hyperbolic decay kinetics models with three parameters. The advantage of using these kinetics models relies on the fact that the maximal sorption capacity can be extrapolated at dripping time zero ($t = 0$). Thus, according to the exponential decay kinetic model, the maximal sorption capacity at $t = 0$ was estimated to be 12.745, 12.034, and 3.447 g/g, for MO-15W, MO-5W, and *n*-dodecane, respectively. In turn, the hyperbolic decay kinetic model suggested higher maximal sorption capacity at $t = 0$, that is, 14.486, 12.896, and 3.501 g/g, for MO-15W, MO-5W, and *n*-dodecane, respectively.

Finally, the advanced recovery (80–92%) of retained oils from the spent composite sorbent was performed by using the centrifugation technique. Also, the Wool-Fe_3O_4-Polysiloxane sorbent demonstrated its ability to be recycled in four cycles of reuse.

Conflicts of interest

Authors have no conflict of interest to declare.

Acknowledgments

Supplementary data

Supporting information for this article is available on the journal's website under https://doi.org/10.5802/crchim.168 or from the author.

References

[1] A. Dhaka, P. Chattopadhyay, *J. Environ. Manage.*, 2021, **288**, article no. 112428.

[2] F. Muttin, *Appl. Ocean Res.*, 2008, **30**, 107-112.

[3] A. Abidli, Y. Huang, P. Cherukupally, A. M. Bilton, C. B. Park, *Environ. Technol. Innovation*, 2020, **18**, article no. 100598.

[4] R. Manivel, R. Sivakumar, *Mater. Today: Proc.*, 2020, **21**, 470-473.

[5] N. Bhardwaj, A. N. Bhaskarwar, *Environ. Pollut.*, 2018, **243**, 1758-1771.

[6] L. M. T. M. Oliveira, J. Saleem, A. Bazargan, J. L. da S. Duarte, G. McKay, L. Meili, *J. Hazard. Mater.*, 2021, **407**, article no. 124842.

[7] B. Doshi, M. Sillanpää, S. Kalliola, *Water Res.*, 2018, **135**, 262-277.

[8] J. Saleem, M. Adil Riaz, M. Gordon, *J. Hazard. Mater.*, 2018, **341**, 424-437.

[9] J. Pinto, A. Athanassiou, D. Fragouli, *J. Environ. Manage.*, 2018, **206**, 872-889.

[10] H. Singh, N. Bhardwaj, S. K. Arya, M. Khatri, *Environ. Nanotechnol. Monit. Manag.*, 2020, **14**, article no. 100305.

[11] K. Qiao, W. Tian, J. Bai, L. Wang, J. Zhao, Z. Du, X. Gong, *J. Taiwan Inst. Chem. Eng.*, 2019, **97**, 227-236.

[12] G. E. Rajaei, S. Khalili-Arjaghi, E. Fataei, N. Sajjadi, M. Kashefi-Alasl, *C. R. Chim.*, 2021, **23**, 563-574.

[13] B. Ge, Z. Zhang, X. Zhu, G. Ren, X. Men, X. Zhou, *Colloids Surf. A: Physicochem. Eng. Asp.*, 2013, **429**, 129-133.

[14] L. Yang, Z. Wang, L. Yang, X. Li, Y. Zhang, C. Lu, *Ind. Crops Prod.*, 2017, **101**, 1-10.

[15] J. Mao, W. Jiang, J. Gu, S. Zhou, Y. Lu, T. Xie, *Appl. Surf. Sci.*, 2014, **317**, 787-793.

[16] L. Yu, G. Hao, J. Gu, S. Zhou, N. Zhang, W. Jiang, *J. Magn. Magn. Mater.*, 2015, **394**, 14-21.

[17] A. Kamgar, S. Hassanajili, *J. Mol. Liq.*, 2020, **315**, article no. 113709.

[18] Q. Wang, Y. Zhang, T. Hu, C. Meng, *Microporous Mesoporous Mater.*, 2019, **278**, 185-194.

[19] P. Madhusudhana Reddy, C. J. Chang, J. K. Chen, M. T. Wu, C. F. Wang, *Appl. Surf. Sci.*, 2016, **368**, 27-35.

[20] J. Hu, J. Zhu, C. Jiang, T. Guo, Q. Song, L. Xie, *Colloids Surf. A: Physicochem. Eng. Asp.*, 2019, **577**, 429-439.

[21] M. Khalilifard, S. Javadian, *Chem. Eng. J.*, 2021, **408**, article no. 127369.

[22] Z. Gao, S. Zhou, Y. Zhou, H. Wan, C. Zhang, B. Yao, T. Chen, *Colloids Surf. A: Physicochem. Eng. Asp.*, 2021, **613**, article no. 126122.

[23] B. Ge, X. Zhu, Y. Li, X. Men, P. Li, Z. Zhang, *Colloids Surf. A: Physicochem. Eng. Asp.*, 2015, **482**, 687-692.

[24] B. Song, J. Zhu, H. Fan, *Mar. Pollut. Bull.*, 2017, **120**, 159-164.

[25] C. Cojocaru, P. P. Dorneanu, A. Airinei, N. Olaru, P. Samoila, A. Rotaru, *J. Taiwan Inst. Chem. Eng.*, 2017, **70**, 267-281.

[26] P. P. Dorneanu, C. Cojocaru, N. Olaru, P. Samoila, A. Airinei, L. Sacarescu, *Appl. Surf. Sci.*, 2017, **424**, 389-396.

[27] S. Cao, T. Dong, G. Xu, F. Mei Wang, *J. Nat. Fibers*, 2017, **14**, 727-735.

[28] B. C. Condurache, C. Cojocaru, P. Samoila, M. Ignat, V. Harabagiu, *Int. J. Environ. Sci. Technol.*, 2022, **19**, 367-378.

[29] C. Cojocaru, L. Pricop, P. Samoila, R. Rotaru, V. Harabagiu, *Polym. Test.*, 2017, **59**, 377-389.

[30] P. Samoila, L. Sacarescu, A. I. Borhan, D. Timpu, M. Grigoras, N. Lupu, M. Zaltariov, V. Harabagiu, *J. Magn. Magn. Mater.*, 2015, **378**, 92-97.

[31] P. Samoila, C. Cojocaru, E. Mahu, M. Ignat, V. Harabagiu, *J. Environ. Chem. Eng.*, 2021, **9**, article no. 104961.

[32] Y. P. Yew, K. Shameli, M. Miyake, N. Kuwano, N. B. Bt Ahmad Khairudin, S. E. Bt Mohamad, K. X. Lee, *Nanoscale Res. Lett.*, 2016, **11**, 1-7.

[33] M. Filippousi, M. Angelakeris, M. Katsikini, E. Paloura, I. Efthimiopoulos, Y. Wang, D. Zamboulis, G. Van Tendeloo, *J. Phys. Chem. C*, 2014, **118**, 16209-16217.

[34] J. A. Fuentes-García, A. Carvalho Alavarse, A. C. Moreno Maldonado, A. Toro-Córdova, M. R. Ibarra, G. F. Goya, *ACS Omega*, 2020, **5**, 26357-26364.

[35] H. Hammani, M. El Achaby, K. El Harfi, M. A. El Mhammedi, A. Aboulkas, *C. R. Chim.*, 2020, **23**, 589-606.

[36] Y. Zhang, W. Huang, C. Hayashi, J. Gatesy, J. McKittrick, *J. R. Soc. Interface*, 2018, **15**, article no. 20180093.

[37] Z. Zhao, C. Song, J. Zhou, R. Hu, H. Xiao, Y. Liu, M. Lu, *J. Appl. Polym. Sci.*, 2020, **137**, 1-11.

[38] B. Fernández-d'Arlas, *Eur. Polym. J.*, 2018, **103**, 187-197.

[39] P. Taylor, B. A. Trofimov, L. M. Sinegovskaya, N. K. Gusarova, *J. Sulfur. Chem.*, 2009, **30**, 518-554.

[40] A. Bazargan, J. Tan, G. McKay, *J. Test. Eval.*, 2015, **43**, 1271-1278.

[41] A. Bazargan, H. Sadeghi, R. Garcia-Mayoral, G. McKay, *J. Colloid Interface Sci.*, 2015, **450**, 127-134.